

---

# AN EVALUATION OF BAYESIAN METHODS FOR BATHYMETRY-BASED LOCALIZATION OF AUTONOMOUS UNDERWATER ROBOTS

---

A PREPRINT (v1) OF ICRA 2019 SUBMISSION

**Jungseok Hong\*, Michael Fulton, and Junaed Sattar**

Department of Computer Science and Engineering  
University of Minnesota Twin Cities  
Minneapolis, MN, 55455, USA

{<sup>1</sup>jungseok, <sup>2</sup>fulto081, <sup>3</sup>junaed} at umn.edu

## ABSTRACT

This paper presents novel probabilistic algorithms for localization of autonomous underwater vehicles (AUVs) using bathymetry data. The algorithms, based on the principles of the Bayes filter, work by fusing bathymetry information with depth and altitude data from an AUV. Four different Bayes filter-based algorithms are used to design the localization algorithms: the Extended Kalman Filter (EKF), Unscented Kalman Filter (UKF), Particle Filter (PF), and Marginalized Particle Filter (MPF). The goal is to have these four filters available for localization under different bathymetric conditions and available computational resources. The localization algorithms overcome unique challenges of the underwater domain, such as visual distortion and RF signal attenuation, which make landmark-based localization infeasible. We evaluate the accuracy and computational cost of the algorithms in a range of simulations that use real-world bathymetry data under different operating conditions.

**Keywords** Underwater localization · Bathymetry-based AUV localization · Low-cost localization

## 1 Introduction

The field of underwater robotics has been experiencing significant development of late, primarily driven by active research in AUVs. AUVs have seen applications in environmental monitoring (*e.g.*, [1, 2, 3]), bathymetry surveys [4], and security [5], among others. For AUVs to navigate and operate such missions successfully, the ability to *localize* accurately is a must-have. However, localization underwater is a challenging and open problem due to the unique circumstances AUVs face: GPS and other forms of radio frequency (RF)-based communications are either completely unavailable or limited to extremely small ranges, and landmarks are often undetectable by exteroceptive sensors. Our work in this paper presents a novel, low-cost approach for localizing AUVs in water bodies for which bathymetry information is available.

The AUV localization problem, in fact for all domains, has been studied extensively. In a broad sense, there are primarily three major techniques to address the problem for underwater robots: using inertial data combined with dead reckoning [6], acoustic transponders [7], and landmark-based (also known as *geophysical* features) approaches (*e.g.*, [8, 9]). The first of these use the measurements from an inertial measurement unit (IMU) and some form of velocity measurement (*e.g.*, from a Doppler velocity log (DVL)) to estimate the position of the robot by correcting the IMU's drift with DVL information. This approach, while widely adopted, often struggles with drifts over time and expensive, high-accuracy IMUs are required (*e.g.*, [10, 11, 12]). The techniques using acoustic transponders include long baseline (LBL) [13], ultra-short baseline (USBL) [14], and short baseline (SBL). However, most of these techniques require either a surface ship to carry a *transponder* or pre-installed beacons on the floor of the water body in question. In many

---

\*The authors are with the Department of Computer Science and Engineering, University of Minnesota Twin Cities, 200 Union St SE, Minneapolis, MN, 55455, USA

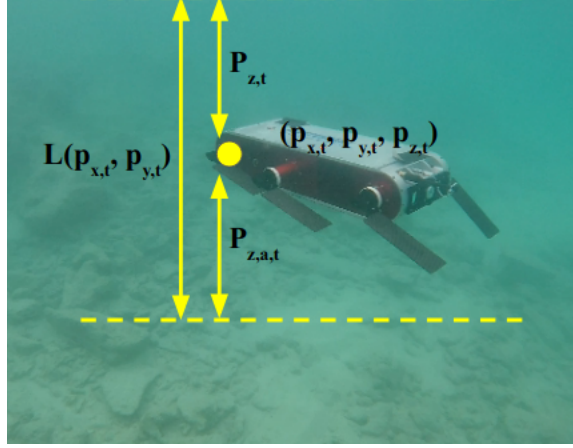


Figure 1: Visual representation of AUV location in a body of water. The top of the figure is assumed to be the surface, which is indicated by the dashed yellow line.

applications, it is impractical to install these devices for localization purposes because of the added cost and associated overhead. Lastly, landmark-based methods use visual and acoustic sensors to detect known features in the marine environment, usually on the floor, and the AUVs can localize themselves relative to such landmarks. However, optical distortions such as scattering, absorption, and attenuation (*e.g.*, arising from turbidity in the water) can be extreme which results in visual features only being visible up close. This makes it challenging to use vision-based methods for broad area localization. As such landmark-based methods with an acoustic sensor provide pragmatic means to tackle underwater localization problems. This, however, requires prior information on the topology of the water body, and in most circumstances, this is available as bathymetry data.

Bathymetry data can assist in AUV localization for each  $(x, y)$  grid location on the surface of the water body where depth information is available. However, once underwater, the bathymetry data at a given grid location varies with the depth of the robot itself, thus an AUV would need both a depth sensor and a bottom sounder or altimeter to make use of this information. The eventual goal is to infer the robot's position  $(x, y, z)$  and orientation  $(\phi, \theta, \xi)$  in 6-DOF with respect to the body of water. Localization using bathymetry maps generally uses a form of the Bayes filter algorithm to estimate these *state variables* [15]. The Bayes filter [16] provides a measure of *belief* representing knowledge about the state of the AUV under a Markovian assumption. However, while it provides an optimal solution, it is often intractable to compute.

In this paper, we developed and implemented underwater localization algorithms for water bodies with bathymetry data, taking depth data from a pressure sensor and the altitude data from a single-beam sonar as input, by using four Bayes filter-based methods: EKF, UKF, PF, and MPF. The EKF and UKF are the parametric implementations of the Bayes filter algorithm with Gaussian assumptions, and PF is a nonparametric implementation. MPF, otherwise known as the Rao-Blackwellized Particle Filter (RBPF), is a hybrid algorithm that combines Kalman Filter (KF) and PF [17].

The main contributions of this paper are the following:

- Provide localization algorithms to estimate the the position of the AUV along all three axes  $(x, y, z)$ ,
- Propose low-cost underwater AUV localization algorithms which work with bathymetry data, and
- Evaluate the performance of four localization algorithms with real-life bathymetric data and different motion models.

## 2 Related Work

Underwater localization using landmark-based methods with acoustic sensors has been widely studied. For these methods, ranging-type sonar including the single-beam, profiling, and multi-beam variety have been used [9]. Multi-beam and profiling sonars collect multiple measurements, and they can give more accurate results than a single-beam sonar. Fairfield and Wettergreen [18] used PF with a multi-beam sonar to localize an AUV. Ura et al. [19] used a profiling sonar with PF to estimate a two-dimensional  $(x, y)$  vehicle state, but not along the depth  $(z)$  axis. Nakatani et al. [20] adopted a profiling sonar with PF, also expressing vehicle state with  $(x, y)$  positions. Although multi-beam and profiling sonar-based methods yield better results, such sensors can be prohibitively expensive.

A single-beam sonar uses a narrow beam to measure the altitude, and it is vulnerable to defective measurements. However, it has been widely adopted to solve localization problems since it is the cheapest type of sensor among the acoustic sensors [12]. Williams and Mahon [21] used a single-beam sonar with PF and, the states that have  $(x, y, z)$  positions and their velocities. Meduna et al. [22] used a single-beam sonar with a point mass filter (PMF) and  $(x, y)$  positions. Kim and Kim [23] used a single-beam sonar with MPF along with the states that have  $(x, y, z)$  positions; their velocities; and roll, pitch, and yaw angles, but they assumed that they can accurately measure all the 6-DOF information from an IMU which is often not possible or requires expensive, high-end IMUs.

Along with the data from a sonar, several Bayes filter-based methods have been used to solve the localization problem [24]. Among Bayes filters, EKF and UKF have seen the most use in this domain (e.g., [25, 26]). Karimi et al. [11] shows that EKF can outperform UKF in their particular case. However, UKF captures up to second-order non-linearities in the state transition process [9], which in theory could outperform an EKF in similar applications. We thus develop both EKF and UKF-based algorithms and compare their performance in AUV localization. Although EKF and UKF can handle unimodal Gaussian distributions, they often fail to converge when the underlying distribution is multi-modal in nature. The inherent nonlinearity of the underwater terrain or nonlinear AUV motions underwater makes it challenging for these methods to work reliably. To address such issues, PF has been widely used (e.g., [27, 19, 20, 28, 29]). However, PF is computationally expensive, and thus can be prohibitive to run on-board AUVs for real-time localization. MPF is computationally less expensive but provides similar benefits to a full PF, handling nonlinearity to some extent [17], making it possible to be used in underwater localization (e.g., [30, 23]). However, localization with bathymetry data considering 3-DOF states and using four Bayes filter-based algorithms (EKF, UKF, PF, and MPF) is yet to be extensively studied.

### 3 Problem Formulation

#### 3.1 General model

A general discrete time state-space model can be represented as Eq. 1 to formulate the localization problem where  $x_t$  is a state,  $u_t$  is a control input, and  $y_t$  is a measurement.  $f$  and  $h$  can be either linear or nonlinear functions.  $q_t$  and  $r_t$  represent the noise from movements and measurements. The model in Eq. 1 is used for EKF, UKF, and PF. The model for MPF is introduced later in this section.

$$\begin{cases} x_t = f(x_{t-1}, u_t) + q_t \\ y_t = h(x_t) + r_t \end{cases} \quad (1)$$

The state and control input are defined as follows:

$$x_t = [p_{x,t} \quad p_{y,t} \quad p_{z,t}]^T \quad (2)$$

$$u_t = [v_{x,t} \quad v_{y,t} \quad v_{z,t}]^T \quad (3)$$

The AUV motion models are defined in Eq. 4 and 5.

##### 3.1.1 Linear motion model

All state variables are updated linearly.

$$f(x_t, u_t) = x_t + u_t * dt \quad (4)$$

##### 3.1.2 Linear/Nonlinear mixed motion model

The state variables  $p_{x,t}$  and  $p_{y,t}$  are updated based on the depth of the position  $(p_{x,t}, p_{y,t})$ . When the depth is shallower, the change in motion becomes smaller. The state variable  $p_{z,t}$  is updated linearly like in the linear motion model.

$$f(x_t, u_t) = \begin{bmatrix} p_{x,t} + a \left( \frac{L(p_{x,t}, p_{y,t})}{a_d} + a_{off} \right) * dt \\ p_{y,t} + b \left( \frac{L(p_{x,t}, p_{y,t})}{b_d} + b_{off} \right) * dt \\ p_{z,t} + v_{z,t} * dt \end{bmatrix} \quad (5)$$

where  $a$ ,  $a_d$ ,  $a_{off}$ ,  $b$ ,  $b_d$ , and  $b_{off}$  are constants for each water body.  $L(p_{x,t}, p_{y,t})$  is the height of each water body at position  $(p_{x,t}, p_{y,t})$ .

### 3.1.3 Measurement model

The measurement function  $h$  is the same for both the linear model and the mixed model.

$$h(x_t) = [p_{z,t} \quad L(p_{x,t}, p_{y,t}) - p_{z,t}]^T \quad (6)$$

$p_{z,t}$  represents the depth of the vehicle from the surface measured by the pressure sensor, and  $p_{z,a,t}$  represents the altitude of the AUV measured by the single-beam sonar. Therefore, the sum of  $p_{z,t}$  and  $p_{z,a,t}$  is the height  $L(p_{x,t}, p_{y,t})$  at the position  $p_{x,t}, p_{y,t}$  as shown in Fig. 1. For the rest of this paper, the term *height* will refer to the total depth of the water body from the floor to the surface.

### 3.2 Model for MPF

In order to apply MPF [17], the model in Eq. 1 is separated into linear and nonlinear state variables as shown in Eq. 7 and 8. The motion model noise  $q_t^n, q_t^l$ , and the measurement model noise  $r_t$  are assumed to be Gaussian with zero mean.

$$x_t = \begin{bmatrix} x_t^n \\ x_t^l \end{bmatrix} \quad (7)$$

$$\begin{cases} x_{t+1}^n = f_t^n(x_t^n) + A_t^n(x_t^n)x_t^l + G_t^n(x_t^n)q_t^n \\ x_{t+1}^l = f_t^l(x_t^n) + A_t^l(x_t^n)x_t^l + G_t^l(x_t^n)q_t^l \\ y_t = h_t(x_t^n) + C_t(x_t^n)x_t^l + r_t \end{cases} \quad (8)$$

## 4 Methodology

Since the motion model in Eq. 5 and the measurement model in Eq. 6 have nonlinearity, it is necessary to use nonlinear Bayes filter algorithms to solve the localization problem. EKF and UKF are widely used to handle nonlinear state estimation with the assumption that the state variables follow the Gaussian distribution. However, they do not always perform well when the state estimation involves non-Gaussian distributions [31]. The PF [32] is resilient to various types of noise, but it is computationally expensive. MPF combines PF and EKF and it sacrifices efficiency. However, it has been shown to work well.

### 4.1 Extended Kalman Filter

In order to linearize a nonlinear system, EKF takes the first order of the Taylor series expansion [16]. Linear matrices in KF are replaced with Jacobians to make predictions. EKF consists of two parts: the prediction step and the correction step. EKF first predicts the state using a motion model. Once the measurements are acquired, EKF updates the state prediction using the measurements. It is assumed that the state follows a Gaussian distribution with one mode. Due to this assumption, EKF is computationally efficient and each update takes  $O(d^3)$  where  $d$  is the dimension of the state  $x_t$  [33]. EKF is directly applied to Eq. 1 for linear and mixed motion cases.

### 4.2 Unscented Kalman Filter

UKF [16] is another approach to linearize a nonlinear system using an unscented transform instead of the Taylor series. UKF chooses  $2n + 1$  sigma points from the Gaussian distribution, and they are passed through the motion model  $f$  where  $n$  is the number of dimensions. Free parameters  $\alpha, \beta$ , and  $\kappa$  decide the distribution of the sigma points which are used to approximate Gaussian distributions. After this, UKF approximates a Gaussian distribution with the sigma points. In this way, UKF can create a more accurate approximation of the Gaussian distribution than EKF. Since the estimation is based on the Gaussian distribution assumption, it may not work for the multi-modal distributions. In most cases, UKF shows notable improvements compared to EKF. The computational complexity of UKF is close to EKF [33]. UKF is also directly applied to Eq. 1 for linear and mixed motion cases.

### 4.3 Particle filter

PF [34] implements the Bayes filter algorithm using sequential Monte Carlo methods. Unlike EKF and UKF, PF does not require any assumptions regarding the distribution. Rather, it uses  $N$  particles to approximate the distribution of the state  $x_t$ . The more particles there are, the more accurate the approximation of the distribution. Furthermore, it can handle distributions with high nonlinearity and multiple modes. However, the computational complexity increases as  $N$

---

**Algorithm 1** Depth-based PF Localization

---

```
1: D-PFL main
2:  $L$  = Target lake
3:  $N$  = The number of particles
4:  $x_{init}$  = Initial pose of a robot
5:  $x_1$  = Initialize_around_pose( $L, N$ )
6:  $z_t$  = Sensor measurements.
7:  $u_t$  = Control input
8: for  $t = 1, \dots, T$  do
9:    $x_p = x_t$ 
10:   $x_t, w_t$  = PFL_update( $L, x_p, u_t, z_t, rand\%$ )
11:   $est\_pose$  = PFL_get_pose( $x_t, w_t$ )
12: end for
13: return  $est\_pose$ 
```

---

---

**Algorithm 2** PF Localization Update

---

```
1: PFL_update( $L, x_p, u_t, z_t, rand\%$ )
2: for  $m = 1, \dots, N$  do
3:    $x(m, :) = \text{motion\_update}(u_t, x_p(m, :), L)$ 
4:    $w(m) = \text{sensor\_update}(z_t, x(m, :), L)$ 
5: end for
6:  $w_{total} = \text{sum}(w)$ 
7: for  $m = 1, \dots, N$  do
8:    $w(m) = w(m)/w_{total}$ 
9: end for
10:  $x_t = \text{resample\_particles}(x(m, :), w, L, rand)$ 
11:  $w_t = w$ 
12: return  $x_t, w_t$ 
```

---

grows. The computational complexity of PF for each update is  $O(Nd^2)$ . When  $N$  is much larger than  $d$ , PF can be much slower than EKF and UKF [35]. This is often the main drawback of PF for a real-time implementation.

A depth-based PF localization (d-PFL) algorithm was proposed and is shown in Algorithm 1. **PFL\_update()** takes a bathymetry map, measurements, and control inputs and returns propagated particles and their weights as shown in Algorithm 2. In order to evaluate weights  $w_t$ , the multivariate Gaussian distribution is used as shown in Eq. 9.

$$w_t = w_{t-1} e^{-\frac{1}{2}(x-\mu)^T \Sigma^{-1}(x-\mu)} \quad (9)$$

During the update process, the algorithm only assigns weights if the particle is within the boundaries of the map. Once the weights for the particles are calculated, they are normalized to ensure that they sum to 1. Then, particles are resampled based on their weights. In order to avoid a situation where all the particles are trapped in incorrect positions in similar environments, only parts of the  $N$  particles are sampled randomly at each time step. Although this can degrade the accuracy of the algorithm, it decreases the chance of incorrect estimation occurrences. Once **PFL\_update()** returns the propagated particles along with the corresponding weights, the pose of the AUV is estimated using Eq. 10.

$$\hat{x} = \sum_{m=1}^M w^{[m]} x^{[m]} \quad (10)$$

#### 4.4 Marginalized Particle filter

MPF was proposed to reduce the computational complexity while retaining a similar performance when the model has a linear substructure [31]. The core idea of MPF is to marginalize linear state(s) from the state vector and use KF to estimate the linear state(s). PF is then used to estimate the remaining nonlinear state(s). The computational complexity of MPF is defined in [36] and can be simplified to  $O(d_n^3 N)$  for our case where  $d_n$  is the dimension of the nonlinear state(s).

---

**Algorithm 3** MPF

---

```
1: Initialize particles
2:   Initialize nonlinear state variables
3:   Initialize linear state variables
4: for  $t = 1, \dots, T$  do
5:   PF measurement update
6:     Evaluate the weights
7:     Estimate nonlinear state variables
8:     Resample particles
9:   KF measurement update
10:    Estimate linear state variables
11:  PF prediction
12:    Propagate nonlinear state variables
13:  KF prediction
14:    Propagate linear state variables
15: end for
```

---

In our case, the ratio  $\frac{N(k)}{N_{PF}}$  is 1.1 where  $N(k)$  is the number of particles that can be used for MPF, and  $N_{PF}$  is the number of particles used for the standard PF. The ratio means that MPF can use 10% more particles than PF while having the same computational complexity as the standard PF. However, EKF and UKF are still faster than MPF albeit less accurate.

The MPF localization algorithm is shown in Algorithm 3:

#### 4.4.1 Initialization of particles

Nonlinear state variables and linear state variables are separately initialized as shown in Eq. 11 and 12.

$$x_{0|-1}^{n,(i)} \sim p(x_0^n) \quad (11)$$

$$\{x_{0|-1}^{l,(i)}, P_{0|-1}^{(i)}\} = \{\bar{x}_0^l, \bar{P}_0\} \quad (12)$$

#### 4.4.2 PF measurement update

The weight for each particle is updated using the likelihood in Eq. 13, and the normalized weights are used to estimate the nonlinear state. Lastly, the particles are resampled based on the weights.

- Evaluation of the weight of a particle  $i$  at time  $t$  and normalization to  $\tilde{w}_t^{(i)}$  :

$$w_t^{(i)} = p(y_t | X_t^{n,(i)}, Y_{t-1}) \quad (13)$$

$$p(y_t | X_t^n, Y_{t-1}) = \mathcal{N}(h_t + C_t \hat{x}_{t|t-1}^l, C_t P_{t|t-1} C_t^T + R_t) \quad (14)$$

- Estimation of nonlinear state variables:

$$\hat{x}_{t|t}^n = \sum_{i=1}^N w_t^{(i)} x_{t|t-1}^{n,(i)} \quad (15)$$

- Resampling of particles:

$$Pr(x_{t|t}^{n,(i)} = x_{t|t-1}^{n,(j)}) = \tilde{w}_t^{(j)} \quad (16)$$

#### 4.4.3 KF measurement update

KF is used to correct error using the measurements and estimate the linear state.

- Measurement update:

$$M_t = C_t P_{t|t-1} C_t^T + R_t \quad (17)$$

$$K_t = P_{t|t-1} C_t^T M_t^{-1} \quad (18)$$

$$x_{t|t}^{l,(i)} = x_{t|t-1}^{l,(i)} + K_t(y_t - h_t - C_t \hat{x}_{t|t-1}^l) \quad (19)$$

$$P_{t|t} = P_{t|t-1} - K_t M_t K_t^T \quad (20)$$

- Estimation of linear state variables:

$$\hat{x}_{t|t}^l = \sum_{i=1}^N w_t^{(i)} x_{t|t}^{l,(i)} \quad (21)$$

#### 4.4.4 PF prediction

PF predicts the states of the propagated particles using the nonlinear motion model the same way as the standard PF using the results from the PF measurement update step.

- Propagation of nonlinear state variables:

$$x_{t+1|t}^{n,(i)} \sim p(x_{t+1|t}^n | X_t^{n,(i)}, Y_t) \quad (22)$$

#### 4.4.5 KF prediction

The results from the KF measurement update step are combined in this step to estimate the states of the propagated particles.

- Propagation of linear state variables:

$$N_t = A_t^n P_{t|t} (A_t^n)^T + G_t^n Q_t^n (G_t^n)^T \quad (23)$$

$$L_t = \bar{A}_t^l P_{t|t} (A_t^n)^T N_t^{-1} \quad (24)$$

$$\begin{aligned} \hat{x}_{t+1|t}^l &= \bar{A}_t^l \hat{x}_{t|t}^l + G_t^l (Q_t^{ln})^T (G_t^n Q_t^n)^{-1} z_t \\ &\quad + f_t^l + L_t (z_t - A_t^n \hat{x}_{t|t}^l) \end{aligned} \quad (25)$$

$$P_{t+1|t} = \bar{A}_t^l P_{t|t} (\bar{A}_t^l)^T + G_t^l \bar{Q}_t^l (G_t^l)^T - L_t N_t L_t^T \quad (26)$$

$$z_t = x_{t+1}^n - f_t^n \quad (27)$$

$$\bar{A}_t^l = A_t^l - G_t^l (Q_t^{ln})^T (G_t^n Q_t^n)^{-1} A_t^n \quad (28)$$

$$\bar{Q}_t^l = Q_t^l - (Q_t^{ln})^T (Q_t^n)^{-1} Q_t^{ln} \quad (29)$$

## 5 Experimental Setup and Results

### 5.1 Bathymetry data

The following lakes located in Minneapolis, MN, USA were chosen: Lake Bde Maka Ska, Lake Nokomis, Lake Hiawatha, and Lake Harriet. The lakes were picked since they are large, well-studied, have a non-flat floor, and are easy to access for future field studies. The bathymetry data was acquired from the Minnesota Department of Natural Resources (DNR) [37]. The grid size of the data is mostly 5m, but in some cases the grid size is 10m. The lake depth at each position is in feet, and it is converted to meters for our study. In our experiments, we assumed that the grid size is 1m to simplify the calculations, and the bathymetry data was scaled accordingly.

## 5.2 Simulation Parameters

The linear and mixed models are designed and simulated to evaluate the performance of the localization algorithm using the four filters. Table 1 includes the model parameters for the simulation.

Parameter	Value			
No. of particles for PF, $N_{PF}$	1000			
No. of particles for MPF, $N_{MPF}$	50			
Motion noise cov., $Q$ (m)	0.01	$v_x^2$	0	0
		0	$v_y^2$	0
		0	0	$(0.3048v_z)^2$
Measurement noise cov., $R$ (m)		$0.3048^2$	0	
		0	$0.3048^2$	
Initial uncertainty cov., $P$ (m)		$1^2$	0	0
		0	$1^2$	0
		0	0	$0.3048^2$

Table 1: Model parameters

The input commands for each case and each lake were separately designed due to the lakes' different sizes and depths. In Table 2, the parameters are defined for the linear motion in Eq. 3 and 4 and the mixed motion in Eq. 5. For the mixed model,  $x$  and  $y$  are nonlinear states, and  $z$  is a linear state.

Linear Motion Parameters							
Lake	$v_x(m/s)$	$v_y(m/s)$	$v_z(m/s)$	$a$	$b$		
Bde Maka Ska	1	-3	-0.1524	-0.02	0.06		
Nokomis	2	-4	-0.1524	-0.1	0.2		
Hiawatha	1	2	-0.3048	-0.05	-0.1		
Harriet	1.5	-3	-0.3048	-0.03	0.06		
Nonlinear Motion Parameters							
Lake	$a$	$a_d$	$a_{off}$	$b$	$b_d$	$b_{off}$	$v_z(m/s)$
Bde Maka Ska	0.6	0.2	3	2	10	23	-0.1524
Nokomis	-0.1	0.2	1	1	-1	-1	-0.1524
Hiawatha	-0.05	-0.1	1	1	0	0	-0.3048
Harriet	-0.1	0.2	3	3	1	1	-0.3048

Table 2: Motion parameters

## 5.3 Results and Discussions

For each lake, 100 runs were performed for each filter, and a total of 1,600 runs were conducted. The results are summarized in Table 3 and 4 for each case. One run in Lake Bde Maka Ska is shown in Fig. 2. For both the linear and nonlinear cases, EKF shows the worst performance. UKF performed well in the linear case, but it deviated from the truth in the nonlinear case. It is noticeable that PF and MPF outperform EKF and UKF for both the linear and mixed motion cases.

### 5.3.1 Linear motion case

EKF performed the worst for most lakes and the results are not reliable since the performance varies depending on the given environments. UKF does not always perform best, but it gives reliable and relatively accurate results with lower computational complexity. PF shows the most accurate results for some lakes, but it performs worst for Lake Nokomis. This is likely caused by the fact that Lake Nokomis has a symmetrical structure and less variations in depth. MPF generally gives accurate and reliable results, and it is computationally cheaper than PF. Overall, MPF is the most reliable and accurate filter based on the results. It is worth mentioning that UKF is a good option if the AUV does not have enough computational power and high accuracy is not required. PF can be used for localization if the lake bathymetry has enough variation in depth and has an asymmetrical structure, provided that the AUV has enough computing power.



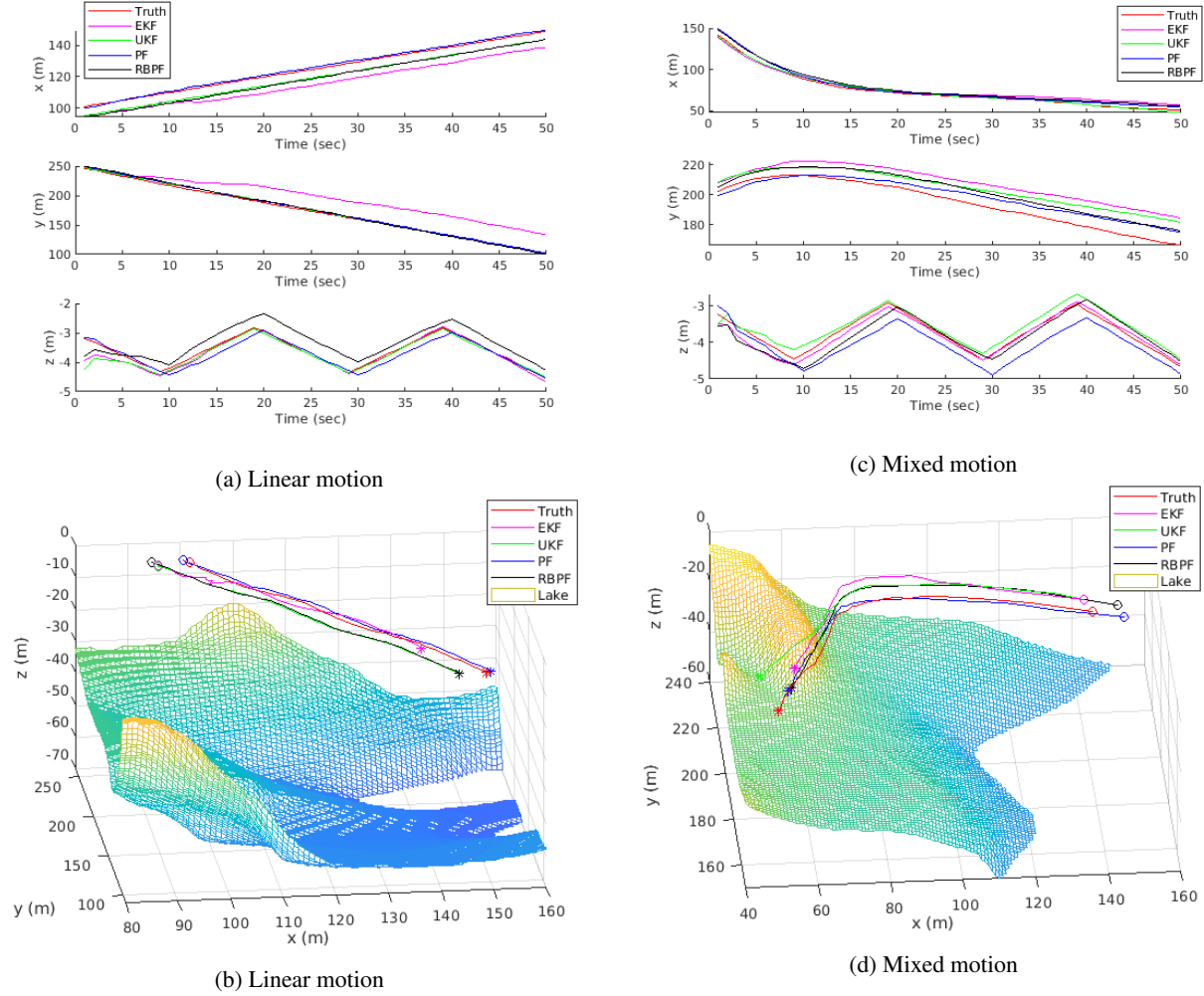


Figure 2: Localization results with Lake Bde Maka Ska using EKF, UKF, PF and MPF approaches (Start:○ End:✱).

### 5.3.2 Nonlinear motion case

Like the linear motion cases, PF and MPF perform better than EKF and UKF. UKF performs the worst for some cases due to the nonlinearity of the motion. PF reveals the same issue that it has in the linear motion cases. Similar to the linear cases, MPF gives reliable and accurate results in general.

### 5.3.3 Discussions

MPF shows the most reliable and accurate results for both the linear and mixed motion cases. If the AUV needs a well-rounded algorithm for the localization problem, MPF is the best filter among the four filters. However, if the bathymetry data of a lake has enough variation, and the task requires high accuracy, then PF is a better option. For an AUV with low computational power, UKF could be the best filter for localization if the linear motion of the AUV is guaranteed.

Lake	Method	$t(s)$	$RMSE_x(m)$	$RMSE_y(m)$	$RMSE_z(m)$
Bde Maka Ska	EKF	50	3.8882	11.4230	0.1507
Bde Maka Ska	UKF	50	3.0045	3.2725	0.1397
Bde Maka Ska	<b>PF</b>	50	<b>1.7842</b>	<b>3.1198</b>	<b>0.3971</b>
Bde Maka Ska	MPF	50	2.9992	2.4574	0.3072
Nokomis	EKF	50	3.5313	4.8192	0.1388
Nokomis	UKF	50	3.2503	3.7075	0.1369
Nokomis	PF	50	13.3850	21.1472	0.3576
Nokomis	<b>MPF</b>	50	<b>3.0372</b>	<b>2.9742</b>	<b>0.2515</b>
Hiawatha	EKF	30	3.0969	3.4106	0.1502
Hiawatha	UKF	30	2.6489	2.9757	0.1605
Hiawatha	<b>PF</b>	30	<b>1.7607</b>	<b>2.6878</b>	<b>0.3655</b>
Hiawatha	MPF	30	2.6116	3.5527	0.2854
Harriet	EKF	30	4.9543	7.9022	0.1882
Harriet	UKF	30	3.0237	3.1416	0.1657
Harriet	PF	30	2.1519	3.6414	0.3536
Harriet	<b>MPF</b>	30	<b>2.7557</b>	<b>2.6160</b>	<b>0.3267</b>

Table 3: Linear motion results

Lake	Method	$t(s)$	$RMSE_x(m)$	$RMSE_y(m)$	$RMSE_z(m)$
Bde Maka Ska	EKF	50	2.3703	3.9278	0.1418
Bde Maka Ska	UKF	50	3.9660	6.1565	0.1559
Bde Maka Ska	<b>PF</b>	50	<b>1.5353</b>	<b>3.0928</b>	<b>0.2042</b>
Bde Maka Ska	MPF	50	2.3750	2.8205	0.1903
Nokomis	EKF	50	4.8618	6.8818	0.1328
Nokomis	UKF	50	13.3273	12.6901	0.1338
Nokomis	PF	50	10.2499	17.6872	0.2967
Nokomis	<b>MPF</b>	50	<b>3.7979</b>	<b>3.6845</b>	<b>0.2336</b>
Hiawatha	EKF	30	3.7730	3.2906	0.1476
Hiawatha	UKF	30	3.3759	3.5925	0.1608
Hiawatha	<b>PF</b>	30	<b>1.3025</b>	<b>2.4465</b>	<b>1.3712</b>
Hiawatha	MPF	30	3.7166	4.0695	0.2807
Harriet	EKF	30	5.2815	9.4283	0.1873
Harriet	UKF	30	4.1619	5.8494	0.1618
Harriet	<b>PF</b>	30	<b>1.4186</b>	<b>2.1306</b>	<b>0.3578</b>
Harriet	MPF	30	3.1695	3.2030	0.3329

Table 4: Mixed motion results

## 6 Conclusion

With bathymetry data and the measurements from a single-beam sonar and pressure sensor, we present four low-cost underwater localization algorithms for AUVs using EKF, UKF, PF, and MPF to compare the performance of each filter for localization in various environments and motions. We considered both the computational complexity and accuracy of each to pick the most suitable filter. The results show that MPF-based localization generally gives the most reliable and accurate results. However, UKF can be a good replacement to PF and MPF at the expense of some accuracy if the AUV only actuates linearly and does not have high computational power. Additionally, PF can achieve the most accurate results when a water body has enough terrestrial variations, and the AUV has enough computational power.

## Acknowledgments

We are thankful to Chelsey Edge, Marc Ho, Jiawei Mo, and Julian Lagman for providing their insight for this study. The Minnesota DNR provided the bathymetric data, and the MnDRIVE Initiative supported this research.

## References

- [1] M. Moline, P. Bissett, S. Blackwell, J. Mueller, J. Sevardjian, C. Trees, and R. Zaneveld, "An autonomous vehicle approach for quantifying bioluminescence in ports and harbors," in *Photonics for Port and Harbor Security*, vol. 5780, pp. 81–88, International Society for Optics and Photonics, 2005.
- [2] D. A. Fong and N. L. Jones, "Evaluation of auv-based adcp measurements," *Limnology and Oceanography: methods*, vol. 4, no. 3, pp. 58–67, 2006.
- [3] A. Forrest, H. Bohm, B. Laval, E. Magnusson, R. Yeo, and M. Doble, "Investigation of under-ice thermal structure: small auv deployment in pavilion lake, bc, canada," in *OCEANS 2007*, pp. 1–9, IEEE, 2007.
- [4] R. J. Huizinga, "Bathymetric and velocimetric surveys at highway bridges crossing the missouri river near kansas city, missouri, june 2–4, 2015," tech. rep., US Geological Survey, 2016.
- [5] S. T. Tripp, "Autonomous underwater vehicles (auvs): a look at coast guard needs to close performance gaps and enhance current mission performance," tech. rep., COAST GUARD RESEARCH AND DEVELOPMENT CENTER GROTON CT, 2006.
- [6] P. A. Miller, J. A. Farrell, Y. Zhao, and V. Djapic, "Autonomous underwater vehicle navigation," *IEEE Journal of Oceanic Engineering*, vol. 35, no. 3, pp. 663–678, 2010.
- [7] P. Batista, C. Silvestre, and P. Oliveira, "A sensor-based controller for homing of underactuated auvs," *IEEE transactions on robotics*, vol. 25, no. 3, p. 701, 2009.
- [8] R. M. Eustice, *Large-area visually augmented navigation for autonomous underwater vehicles*. PhD thesis, Massachusetts Institute of Technology and Woods Hole Oceanographic Institution, 2005.
- [9] L. Paull, S. Saeedi, M. Seto, and H. Li, "Auv navigation and localization: A review," *IEEE Journal of Oceanic Engineering*, vol. 39, no. 1, pp. 131–149, 2014.
- [10] R. Panish and M. Taylor, "Achieving high navigation accuracy using inertial navigation systems in autonomous underwater vehicles," in *OCEANS, 2011 IEEE-Spain*, pp. 1–7, IEEE, 2011.
- [11] M. Karimi, M. Bozorg, and A. Khayatian, "A comparison of dvl/ins fusion by ukf and ekf to localize an autonomous underwater vehicle," in *Robotics and Mechatronics (ICRoM), 2013 First RSI/ISM International Conference on*, pp. 62–67, IEEE, 2013.
- [12] J. Melo and A. Matos, "Survey on advances on terrain based navigation for autonomous underwater vehicles," *Ocean Engineering*, vol. 139, pp. 250–264, 2017.
- [13] A. P. Scherbatyuk, "The auv positioning using ranges from one transponder lbl," in *OCEANS'95. MTS/IEEE. Challenges of Our Changing Global Environment. Conference Proceedings.*, vol. 3, pp. 1620–1623, IEEE, 1995.
- [14] M. Morgado, P. Oliveira, and C. Silvestre, "Experimental evaluation of a usbl underwater positioning system," in *ELMAR, 2010 proceedings*, pp. 485–488, IEEE, 2010.
- [15] T. Y. Teck, M. Chitre, and F. S. Hover, "Collaborative bathymetry-based localization of a team of autonomous underwater vehicles," in *Robotics and Automation (ICRA), 2014 IEEE International Conference on*, pp. 2475–2481, IEEE, 2014.
- [16] S. Thrun, W. Burgard, and D. Fox, *Probabilistic robotics*. MIT press, 2005.
- [17] T. Schon, F. Gustafsson, and P.-J. Nordlund, "Marginalized particle filters for mixed linear/nonlinear state-space models," *IEEE Transactions on signal processing*, vol. 53, no. 7, pp. 2279–2289, 2005.
- [18] N. Fairfield and D. Wettergreen, "Active localization on the ocean floor with multibeam sonar," in *OCEANS 2008*, pp. 1–10, IEEE, 2008.
- [19] T. Ura, T. Nakatani, and Y. Nose, "Terrain based localization method for wreck observation auv," in *OCEANS 2006*, pp. 1–6, IEEE, 2006.
- [20] T. Nakatani, T. Ura, T. Sakamaki, and J. Kojima, "Terrain based localization for pinpoint observation of deep seafloors," in *OCEANS 2009-EUROPE*, pp. 1–6, IEEE, 2009.
- [21] S. Williams and I. Mahon, "A terrain-aided tracking algorithm for marine systems," in *Field and Service Robotics*, pp. 93–102, Springer, 2006.
- [22] D. K. Meduna, S. M. Rock, and R. McEwen, "Low-cost terrain relative navigation for long-range auvs," in *OCEANS 2008*, pp. 1–7, IEEE, 2008.
- [23] T. Kim and J. Kim, "Nonlinear filtering for terrain-referenced underwater navigation with an acoustic altimeter," in *OCEANS 2014-TAIPEI*, pp. 1–6, IEEE, 2014.

- [24] S. Carreno, P. Wilson, P. Ridao, and Y. Petillot, "A survey on terrain based navigation for auvs," in *OCEANS 2010*, pp. 1–7, IEEE, 2010.
- [25] B. He, K. Yang, S. Zhao, and Y. Wang, "Underwater simultaneous localization and mapping based on ekf and point features," in *Mechatronics and Automation, 2009. ICMA 2009. International Conference on*, pp. 4845–4850, IEEE, 2009.
- [26] B.-D. Yoon, H.-N. Yoon, S.-H. Choi, and J.-M. Lee, "Ukf applied for position estimation of underwater-beacon precision," in *Intelligent Autonomous Systems 12*, pp. 501–508, Springer, 2013.
- [27] I. Rekleitis, "A Particle Filter Tutorial for Mobile Robot Localization," Tech. Rep. TR-CIM-04-02, Centre for Intelligent Machines, McGill University, 3480 University St., Montreal, Québec, CANADA H3A 2A7, Jan. 2004.
- [28] R. Karlsson, F. Gustafsson, and T. Karlsson, "Particle filtering and cramer-rao lower bound for underwater navigation," in *Acoustics, Speech, and Signal Processing, 2003. Proceedings.(ICASSP'03). 2003 IEEE International Conference on*, vol. 6, pp. VI–65, IEEE, 2003.
- [29] F. Maurelli, A. Mallios, D. Ribas, P. Ridao, and Y. Petillot, "Particle filter based auv localization using imaging sonar," *IFAC Proceedings Volumes*, vol. 42, no. 18, pp. 52–57, 2009.
- [30] R. Karlsson and F. Gustafsson, "Bayesian surface and underwater navigation," *IEEE Transactions on Signal Processing*, vol. 54, no. 11, pp. 4204–4213, 2006.
- [31] T. B. Schon, R. Karlsson, and F. Gustafsson, "The marginalized particle filter in practice," in *Aerospace Conference, 2006 IEEE*, pp. 11–pp, IEEE, 2006.
- [32] S. Thrun, "Particle filters in robotics," in *Proceedings of the Eighteenth conference on Uncertainty in artificial intelligence*, pp. 511–518, Morgan Kaufmann Publishers Inc., 2002.
- [33] F. Daum, "Nonlinear filters: beyond the kalman filter," *IEEE Aerospace and Electronic Systems Magazine*, vol. 20, no. 8, pp. 57–69, 2005.
- [34] D. Salmond and N. Gordon, "An introduction to particle filters," *State space and unobserved component models theory and applications*, pp. 1–19, 2005.
- [35] F. Gustafsson, "Particle filter theory and practice with positioning applications," *IEEE Aerospace and Electronic Systems Magazine*, vol. 25, no. 7, pp. 53–82, 2010.
- [36] T. B. Schön, R. Karlsson, and F. Gustafsson, "The marginalized particle filter—analysis, applications and generalizations," in *ESAIM: Proceedings*, vol. 19, pp. 53–64, EDP Sciences, 2007.
- [37] N. R. Department, "Lake bathymetric outlines, contours, vegetation, and dem," June 2018.